

AD-A285 142



Dist: A

①

Resonant Tunneling Quantum Well Integrated Optical Waveguide Modulator/Switch

Final Report

AFOSR-TR-94 0573

Grant No. F49620-94-C-0008

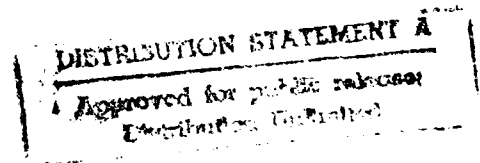
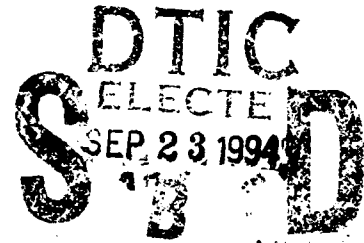
Period of Performance: 12/01/93 - 05/31/94

Presented to:

Air Force Office of Scientific Research
Bolling AFB, DC NE

Presented by:

Physical Optics Corporation
Applied Technology Division
2545 West 237th Street, Suite B
Torrance, CA 90505



Principal Investigator:

Dr. Andrew Kostrzewski
(310) 530-1416

DTIC QUALITY INSURED

July 1994

94-30518



3398

94 9 22 089

DIST: A

| REPORT DOCUMENTATION PAGE | | | Form Approved OMB No. 0704-0188 | |
|--|--|---|---|--|
| Public reporting burden for this collection of information is estimated to average 1 hour per response, including the time for reviewing instructions, searching existing data sources, gathering and maintaining the data needed, and completing and reviewing the collection of information. Send comments regarding this burden estimate or any other aspect of this collection of information, including suggestions for reducing this burden to Washington Headquarters Services, Directorate for Information Operations and Reports, 1215 Jefferson Davis Highway, Suite 1204, Arlington, VA 22202-4302, and to the Office of Management and Budget, Paperwork Reduction Project (0704-0188), Washington, DC 20503. | | | | |
| 1. AGENCY USE ONLY (Leave blank) | 2. REPORT DATE July 31, 1994 | 3. REPORT TYPE AND DATES COVERED Final - 12/01/93 - 05/31/94 | | |
| 4. TITLE AND SUBTITLE Resonant Tunneling Quantum Well Integrated Optical Waveguide Modulator/Switch | | | 5. FUNDING NUMBERS F49620-94-C-0008 | |
| 6. AUTHOR(S) Andrew Kostrzewski, Ph.D | | | 1602/01 | |
| 7. PERFORMING ORGANIZATION NAME(S) AND ADDRESS(ES) Physical Optics Corporation 2545 West 237th Street, Suite B Torrance, California 90505 | | | 8. PERFORMING ORGANIZATION REPORT NUMBER 3246 AFOSR-TR- 94 0573 | |
| 9. SPONSORING / MONITORING AGENCY NAME(S) AND ADDRESS(ES) Air Force Office of Scientific Research / NE Bolling AFB, DC | | | 10. SPONSORING / MONITORING AGENCY REPORT NUMBER F49620-94 C 0008 | |
| 11. SUPPLEMENTARY NOTES | | | | |
| 12a. DISTRIBUTION / AVAILABILITY STATEMENT Approved for public release; distribution unlimited. | | | 12b. DISTRIBUTION CODE A | |
| 13. ABSTRACT (Maximum 200 words) In this Phase I program, Physical Optics Corporation (POC) has investigated resonant tunneling double barrier quantum wells (RTDBQW) for application to all-optical communication networks. The RTDBQW can be used as a building block in superfast SONET/ATM networks. The proposed concept relies on the integration of an optical guided wave modulator with the RTDBQW. Several waveguide modulator architectures have been investigated, including Mach-Zehnder, directional couplers. A Mach-Zehnder interferometer has been selected for the final implementation, and will provide high performance. The major advantage of the proposed integrated optical waveguide modulator/switch is that it uses low voltage, due to the use of the high efficiency RTDBQW diode. This, in turn, increases the theoretical speed limit of the device to the femtosecond regime. One important feature of the RTDBQW device is that its response time is limited by the quantum tunneling time, not by the conventional diode transit time, which leads to the high speed operation. In this Phase I project, POC designed the RTDBQW device, including the optimization and precise definition of the fabricating process to be implemented in Phase II of this program. | | | | |
| 14. SUBJECT TERMS Resonant Tunneling Double Barrier, Quantum Well Diode, Integrated Optics | | | 15. NUMBER OF PAGES 33 | |
| | | | 16. PRICE CODE | |
| 17. SECURITY CLASSIFICATION OF REPORT Unclassified | 18. SECURITY CLASSIFICATION OF THIS PAGE Unclassified | 19. SECURITY CLASSIFICATION OF ABSTRACT Unclassified | 20. LIMITATION OF ABSTRACT SAR | |

TABLE OF CONTENTS

| | | |
|-----|---|----|
| | SF 298 FORM..... | i |
| 1.0 | INTRODUCTION | 1 |
| 2.0 | BACKGROUND OF THE RESONANT TUNNELING DOUBLE BARRIER QUANTUM WELL INTEGRATED OPTICAL WAVEGUIDE MODULATOR | 3 |
| 2.1 | Resonant Tunneling Double Barrier Quantum Well Diode Characteristic..... | 4 |
| 2.2 | Index Modulation Through Negative Plasma Effect of Free Carriers | 7 |
| 3.0 | CHANNEL WAVEGUIDE DESIGN AND OPTIMIZATION..... | 10 |
| 3.1 | Design Of Directional Coupling Mach-Zehnder Interferometer | 13 |
| 4.0 | WAVEGUIDE FABRICATION | 16 |
| 4.1 | Wet Etching Waveguide Fabrication Method..... | 17 |
| 4.2 | Dry Etching Waveguide Fabrication Method | 19 |
| 4.3 | Device Isolation | 21 |
| 4.4 | Contact metal deposition | 23 |
| 4.5 | Pad Metal Deposition..... | 25 |
| 4.6 | Backside Metal Deposition..... | 25 |
| 4.7 | Metal Alloying..... | 25 |
| 4.8 | Post Processing | 25 |
| 5.0 | DEVICE CALIBRATION AND TESTING | 25 |
| 6.0 | POTENTIAL APPLICATIONS | 26 |
| 6.1 | All-Optical Synchronous Multiple Access Networks..... | 26 |
| 7.0 | PHASE I CONCLUSIONS..... | 27 |
| 8.0 | PHASE II RECOMMENDATIONS | 28 |
| 9.0 | REFERENCES | 28 |

| | |
|----------------------|-------------------------------------|
| Accession For | |
| DTIC ORA&I | <input checked="" type="checkbox"/> |
| DTIC TAB | <input type="checkbox"/> |
| Unannounced | <input type="checkbox"/> |
| Justification | |
| By | |
| Distribution/ | |
| Availability Codes | |
| Avail and/or | |
| Dist | |
| A-1 | |

LIST OF FIGURES

| | | |
|----|---|----|
| 1 | POC's electrooptical switch/modulator based on integration of Mach-Zehnder interferometer with a resonant tunneling double barrier quantum well diode. | 2 |
| 2 | Refractive index versus photon energy for AlGaAs material..... | 3 |
| 3 | Schematic conduction-band diagrams of the RTDBQW diode (a) unbiased case (b) biased case. | 5 |
| 4 | Current density of a RTDBQW diode as a function of bias voltage. | 7 |
| 5 | Structure of the proposed diode, with the optical waveguide placed between the emitter and the collector..... | 8 |
| 6 | Refractive index variation versus free charge carriers density | 10 |
| 7 | Dependence of the propagation loss as a function of the free carrier concentration in the AlGaAs ridge waveguide..... | 11 |
| 8 | Waveguide propagation losses of the fundamental mode in the ridge waveguide as a function of the cladding thickness for various waveguide thicknesses..... | 12 |
| 9 | Computer screen showing field distribution for the optimized simple mode waveguide..... | 13 |
| 10 | Schematic diagram of Mach-Zehnder interferometer..... | 14 |
| 11 | P_{out} versus $\Delta\beta/\pi$ characteristics of the Mach-Zehnder interferometer. | 15 |
| 12 | The mask layout used for the fabrication of the Mach-Zehnder interferometer | 16 |
| 13 | Layer structure of the proposed waveguide | 17 |
| 14 | Simulated reflectance of the proposed structure | 26 |
| 15 | The optical data signal is split into N different delay paths..... | 27 |

LIST OF TABLES

| | | |
|---|---|---|
| 1 | Structure of Resonant Tunneling Quantum Well Integrated Optical Waveguide Modulator | 4 |
|---|---|---|

LIST OF FLOW CHARTS

| | | |
|---|---------------------------------------|----|
| 1 | Wet Etching Process | 18 |
| 2 | Dry Etching Process | 20 |
| 3 | Device Isolation Process..... | 22 |
| 4 | Contact Metal Deposition Process..... | 24 |

1.0 INTRODUCTION

One of the most promising technologies for future communications and signal processing is based on optical signal processing. It is inevitable that optical signal processing will play a major role in high speed *all-optical* communication networks, including super-fast SONET/ATM networks (at 10 Gb/s) [1,2]. Most existing network routing schemes rely not on optical data transmission, but rather on electronic routing (switching). This solution is, however, extremely inefficient, especially for high speed communications. In this approach, three operations must be executed to provide data switching:

1. The conversion of the optically represented data stream to an electronic representation;
2. Data switching in the electronic representation;
3. The conversion of the electronic data back to the optical representation for the transmission to the final destination node.

The conversion of the optical signal to electronic and back is costly (the hardware for a high speed transmitter/receiver pair can exceed more than \$5k-\$10k), adding additional cost to an already expensive network. The alternative solution is to perform all of the routing and switching operations without data conversion, such as in an all-optical communication network.

Unfortunately, all-optical routing, however attractive, is still in the early research stage, mostly because of difficulties in providing high speed switching at low cost using all-optical means. In response to the need for all-optical switching and modulators, Physical Optics Corporation (POC) proposed to develop a guided wave EO switch/modulator, which would form a major building block in an opto-electronic integrated circuit (OEIC) to provide the indirect switching/modulation operations that are essential for high speed signal routing and regeneration. POC's design relies on the integration of an optical guided wave switch/modulator with a resonant tunneling double barrier quantum well (RTDBQW) diode [3-7], as shown in Figure 1. Several waveguide geometries have been investigated during this Phase I project, including: (a) a Mach-Zehnder interferometer modulator; (b) a total internal reflection (TIR) switch; (c) a directional coupling modulator; and (d) a cut-off modulator. As a result of our Phase I investigation, we have determined that the final design will be based on Mach-Zehnder interferometer modulator, which provides high performance and is well established. The Mach-Zehnder interferometer [8] architecture was studied in order to optimize the modulation switching efficiency. The phase difference introduced by the RTDBQW will provide high on/off intensity modulation depth.

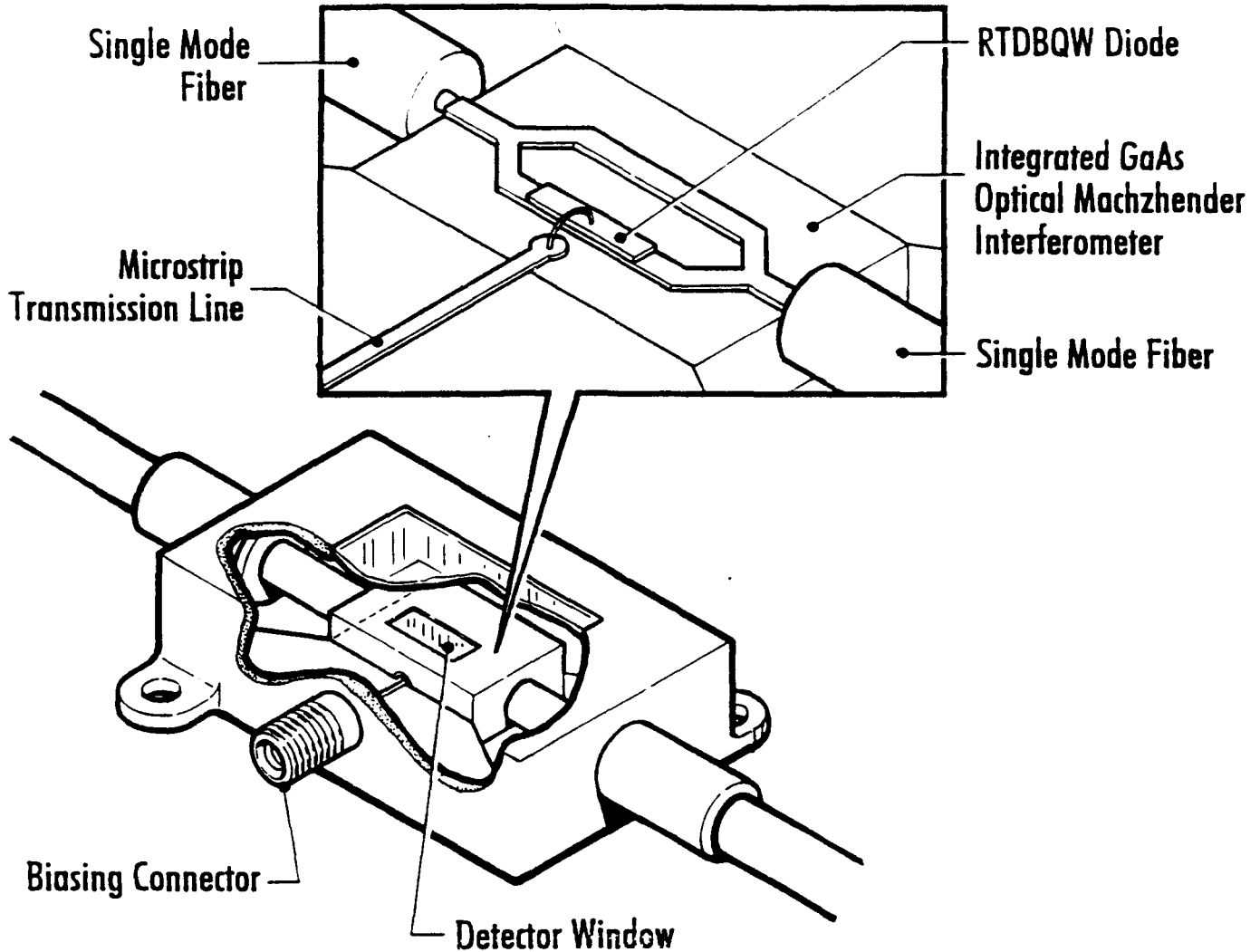


Figure 1
POC's electrooptical switch/modulator based on integration of Mach-Zehnder interferometer with a resonant tunneling double barrier quantum well diode.

The major advantage of the proposed integrated optical waveguide modulator/switch is that it uses low voltage, due to the use of the highly efficient RTDBQW diode. This, in turn, increases the theoretical speed of this device to the *femtosecond regime*, mostly because the response of the device is limited by the quantum tunneling time, not by the conventional diode transit time.

The constraints in the waveguide design and optimization issues imposed by the RTDBQW diode led us to the conclusion that, without a suitable software, this task will be extremely difficult to complete. Initially, our efforts concentrated on finding a commercially available software to perform this task. However, our search was not successful. Fortunately, we developed our own software as part of a Phase II SBIR program entitled "Low Threshold

All-Optical Crossbar Switch on GaAs-GaAlAs Channel Waveguide Array," (Contract No. F49620-92-0047). The resulting software is very flexible, and can be applied to a variety of optical waveguide designs. It offers unlimited interactive CAD and performance verification, which substantially speeds up the design stage of any hybrid structure containing optical waveguides. The program is Microsoft Windows™ compatible, and has a friendly graphical interface and an easy loading procedure. The uniqueness of this software assures us of its commercial value, and POC is planning to make it commercially available in the near future. The software delivers a new tool to all researchers involved in the design and optimization of complicated multilayer waveguide structures. POC will continue the software development effort, upgrading it to provide even more flexibility.

2.0 BACKGROUND OF THE RESONANT TUNNELING DOUBLE BARRIER QUANTUM WELL INTEGRATED OPTICAL WAVEGUIDE MODULATOR

The principle of the proposed waveguide modulator is based on the free carrier plasma effect, where changes in the free carrier density generates a refractive index change. In this program, we determined that the use of a singlemode waveguide was the most optimal solution for this system. The reason for this is that, in order to ensure efficient modulation, the confinement factor of the waveguide should be close to 90%. Since the evanescent wave amplitude must be kept small for low absorption loss, the confinement must be as strong as possible. Thus, the refractive index of the cladding layer must be as small as possible, while the thickness of the waveguide must be as thick as possible. The smallest refractive index for an $\text{Al}_x\text{Ga}_y\text{As}$ system is obtained using AlAs [9]. The refractive indices of AlGaAs materials are calculated and shown in Figure 2, and can be used to design a suitable waveguide structure.

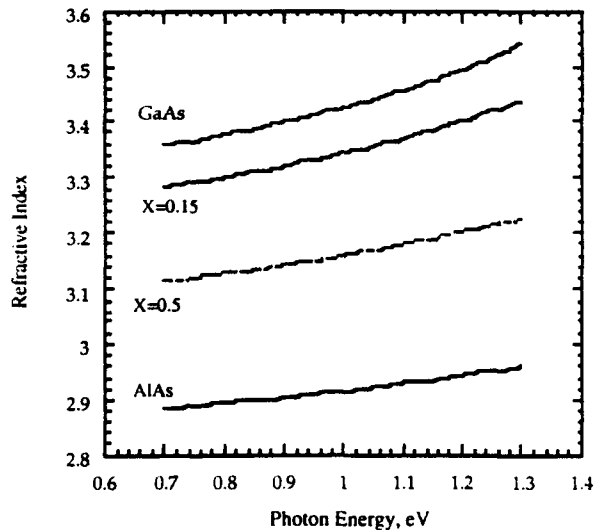


Figure 2
Refractive index versus photon energy for AlGaAs material.

The second consideration of the waveguide modulator is the modulation efficiency, where the thickness of the waveguide cannot be too thick, so that the total carrier change ΔN for index change ∂n is not too high. ΔN is proportional to the product of $\partial N W t$, where ∂N is the carrier density change for refractive index change ∂n , W is the width of the waveguide,

and t is the thickness of the waveguide. This structure is similar to the structure proposed in the Phase I proposal, and is shown in Table 1.

Table 1. Structure of Resonant Tunneling Quantum Well Integrated Optical Waveguide Modulator

| | | |
|----------|--|--|
| 2,000 Å | n ⁺ GaAs | 5E18 (cm ⁻³) |
| 300 Å | I GaAs | 10 ¹³ (cm ⁻³) |
| 35 Å | I AlAs | 10 ¹³ (cm ⁻³) |
| 50 Å | I In _{0.15} Ga _{0.85} As | 10 ¹³ (cm ⁻³) |
| 35 Å | I AlAs | 10 ¹³ (cm ⁻³) |
| 300 Å | I GaAs | 5 x 10 ¹⁷ (cm ⁻³) |
| 800 Å | n ⁺ GaAs | 1E18 (cm ⁻³) |
| 40,000 Å | I GaAs | 10 ¹³ (cm ⁻³) |
| 2,000 Å | I AlAs | 10 ¹³ (cm ⁻³) |
| 13,000 Å | n AlAs | 2E18 (cm ⁻³) |
| 10,000 Å | I GaAs | 2E18 (cm ⁻³) |

There are, however, several changes in our approach. First, the top layer is more heavily doped. There are two reasons for this. One is that the device is a large current device; hence, power consumption must be taken into account. The heavy doping of the top contact layer reduces the contact resistance, and thus reduces the power consumption. The other reason is that the tunneling through the double barrier structure would be easier with an elevated Fermi level at the emission side. Even though the increased doping will increase the material absorption (since the field is mostly concentrated at the AlAs/GaAs side for low refractive index differences), the effective absorption is not going to increase much. The second change is that we made the double barrier structure more or less symmetric for dual direction operations. The third change is that we broke the cladding AlAs layer into two layers: one low doping layer and one high doping layer. The less doped layer provides low absorption loss, while the highly doped layer provides less resistance.

2.1 Resonant Tunneling Double Barrier Quantum Well Diode Characteristic

The resonance tunneling model can be used to describe the principle of operation of the resonant tunneling double barrier quantum well (RTDBQW) diode. In general, a transfer for an electron from the emitter to the well is permitted if the energy of the incoming electron lines up with the energy in the quantum well. If this condition is not satisfied, the transfer will not occur. In the resonant tunneling model, the electrons coming from the emitter are considered as waves propagating through the quantum well. Global transmission can be obtained by performing a summation of all of the multiple scattered waves, due to the barriers in the collector. It is characteristic that the transmission will be

characterized by a sharp peak corresponding to a Fabry-Perot resonance. For other energy levels, two quasi-two-dimensional states exist independently of the Fabry-Perot resonance. Y. Hu and S. Stapleton [10] proved that the summation of all of the multiple scattered waves in the collector is the equivalent of solving the stationary Schrodinger equation. Their proof is based on a simplified model of the double barrier diode (DBD), as shown in Figure 3.

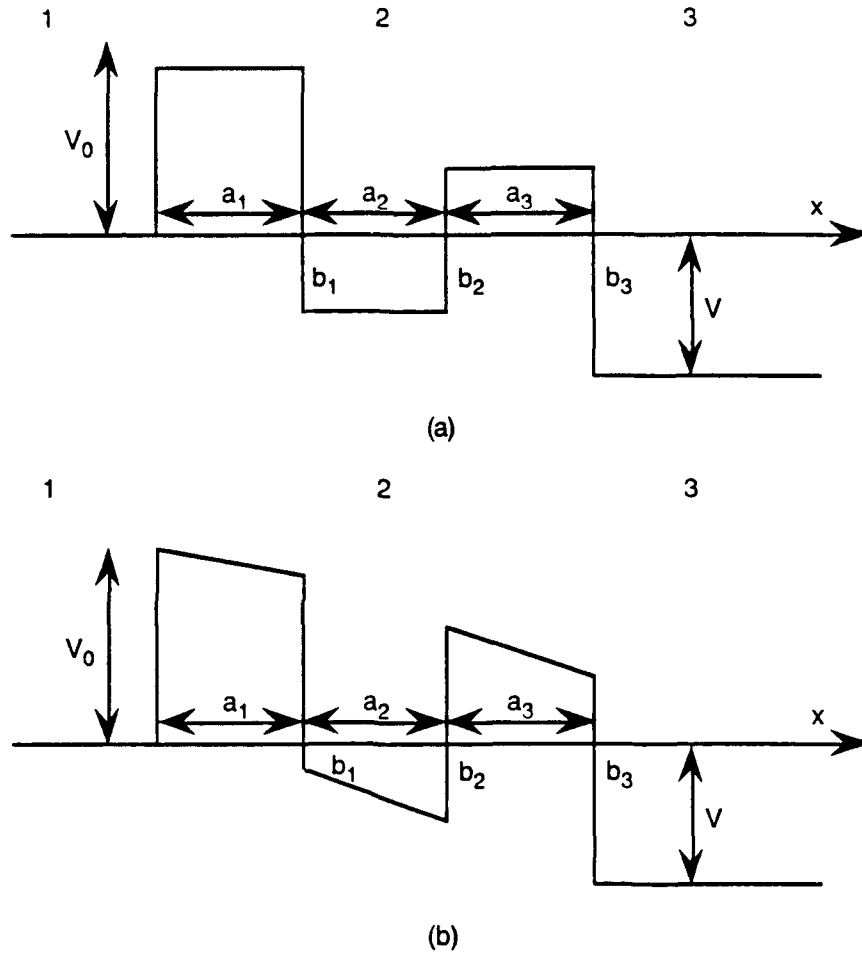


Figure 3
 Schematic conduction-band diagrams of the RTDBQW diode
 (a) unbiased case (b) biased case.

Using the Fabry-Perot model, each quantum well barrier can be characterized by its transmission t and reflection r coefficients. The subscripts l and r indicate the left and right barriers, respectively, while subscripts l and r correspond to waves coming from the left and right sides, respectively.

The summation of all of the transmitted scattered waves can be represented as

$$T = t_{1L}t_{2L}e^{ik_{2x}a_2} \sum_{n=0}^{\infty} \left(r_{1r}r_{2l}e^{i2k_{2x}a_2} \right)^n \quad (1)$$

$$= \frac{t_{1L}t_{2L}e^{jk_{2x}a_2}}{1 - r_{1r}r_{2l}e^{i2k_{2x}a_2}}$$

where k_{jx} ($j = 1, 2, 3$) is the momentum component in the direction of tunneling in the region j .

The global reflected wave can be represented as:

$$R = r_{1l} \frac{t_{1l}r_{2l}t_{1r}e^{i2k_{2x}a_2}}{1 - r_{1r}r_{2l}e^{i2k_{2x}a_2}} \quad (2)$$

Assuming a damped Fabry-Perot model, a damping constant α for the electron waves can be introduced to the last two equations. Thus, the total transmitted and reflected waves are:

$$T = \frac{t_{1l}t_{2l}e^{jk_{2x}a_2 - \alpha a_2}}{1 - r_{1r}r_{2l}e^{i2k_{2x}a_2 - \alpha a_2}} \quad (3)$$

$$R = r_{1l} + \frac{t_{1l}r_{2l}t_{1r}e^{i2k_{2x}a_2 - \alpha a_2}}{1 - r_{1r}r_{2l}e^{i2k_{2x}a_2 - \alpha a_2}} \quad (4)$$

Due to the damping constant, the incoming electron current will be larger than the sum of the transmitted and reflected currents. The difference in the current can be interpreted as the transport of the incoherent electrons into the quantum well. These incoherent electrons will undergo multiple scattering by the barriers, and will finally incoherently tunnel out of the quantum well. If we consider quasi-steady state conditions, these incoherent electrons will form a nonequilibrium distribution in the quantum well, which can be approximated as hot electron distribution. The incoherent current density is zero if the damping coefficient is zero. The opposite situation occurs for a damping coefficient approaching infinity, for which only noncoherent current is present. The total current density for different damping coefficients is shown in Figure 4 [10]. Three damping coefficients have been selected: $\alpha = 0$, $\alpha = 10^6$ and $\alpha = \infty$. This figure is a result of our assumption that all of the incoherent electrons in the quantum well tunnel out through the right barrier.

Figure 4 indicates the changes of differential resistance due to the changes of damping constant α . As $\alpha \rightarrow \infty$, the negative resistance completely disappears and the I-V characteristic is typical to that of a single barrier diode (dotted line in Figure 4).

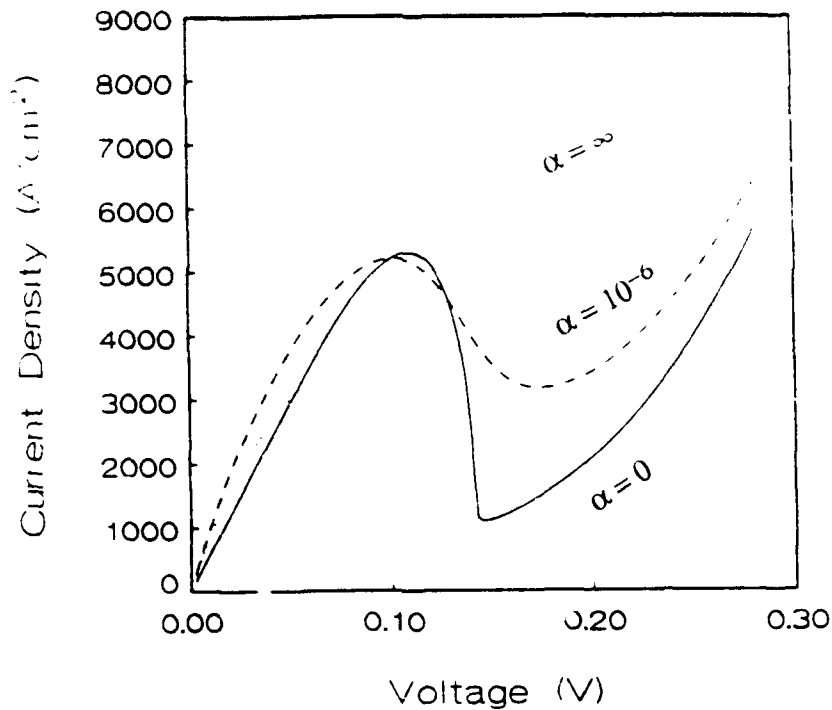


Figure 4

Current density of a RTDBQW diode as a function of bias voltage. These characteristics are superimposed for $\alpha = 0$, $\alpha = 10^6$ and $\alpha = \infty$. This figure has been obtained as a result of the model shown in Figure 3 with following data $a_1=a_2=a_3=50$ Å, barrier height $V_0=0.23$ eV, Fermi energy at the emitter and collector ≈ 0.02 eV, effective mass m_0 in GaAs is 0.067 and GaAlAs $\approx 0.1 m_0$ (m_0 is the free electron mass).

2.2 Index Modulation Through Negative Plasma Effect of Free Carriers

High speed switching and high modulation depths can be obtained for optical signals if a large index modulation can be obtained. The proposed double barrier resonant tunneling diode will provide high current-induced index of refraction modulation. Since current-induced index modulation is much stronger than the linear electro-optic effect, we can make an active device by injecting a time dependent carrier concentration. A very large current density is induced by the resonant tunneling diode. When the optical signal carrier to be modulated is coupled to the ridge waveguide, the induced current will interact with the guided wave using the standard method. The optical waveguide is a part of the diode structure, as shown in Figure 5.

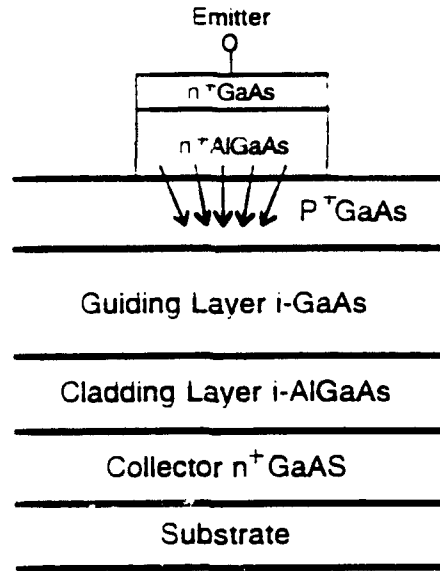


Figure 5
 Structure of the proposed diode, with the optical waveguide placed
 between the emitter and the collector.

The remaining part of this section describes the physical phenomena related to the induced *index of refraction modulation through current injection*.

The motion equation of an electron in an electric field E_y of frequency $\omega/2\pi$ (the frequency of the light to be modulated) along the vector direction of the electric field, y , is

$$m_e^* \frac{dv_y}{dt} = -e \cdot E_y = -e \cdot E \cdot e^{i\omega t} \quad (5)$$

where M_{e^*} is the effective mass of an electron and E_y is the electric field of the optical carrier. The solution for Eq. (5) is

$$V_y = V_{y0} + \frac{ie \cdot E}{\omega \cdot m_e^*} e^{i\omega t} \quad (6)$$

Since the mean velocity without the influence of E_y is 0, the first term V_{y0} is also zero. The current density can be expressed by

$$J_y = NeV_y = \frac{iNe^2 E}{\omega m_e^*} e^{i\omega t} = \sigma \cdot E_y \quad (7)$$

where r is the conductivity. By comparison, r is

$$r = \frac{iNe^2}{\omega m_e^*} \quad (8)$$

The dielectric constant and conductivity enter into the determination of the optical properties of a solid only in the combination [11]:

$$\epsilon(\omega) = N_o^2 + \frac{4\pi i \sigma(\omega)}{\omega} \quad (9)$$

where N_o is the index of refraction without the influence of current. Using Eq. (8), we can easily write Eq. (9) in the following form:

$$\epsilon(\omega) = N_o^2 - \frac{4\pi N e^2}{m_e^* \omega^2} \quad (10)$$

Since the value of the second term in Eq. (10) is much less than N_o^2 , the index of refraction can be written in the following approximate form:

$$n - (\epsilon)^{1/2} \cong n_o \left(1 - \frac{2\pi N e^2}{m_e^* \omega^2 n_o^2} \right) \quad (11)$$

The Δn value in this condition is

$$\Delta n = \frac{-2\pi N e^2}{m_e^* \omega^2 n_o} \quad (12)$$

The refractive index variation versus free charge carriers density is graphically represented in Figure 6.

The change in the index of refraction due to the injected free carriers can be two orders of magnitude higher than that generated by the linear EO effect. Since the length of the proposed device interaction is only on the order of μm , the throughput intensity modulation will be mainly due to refractive index modulation, rather than absorption. This solution can open new possibilities for optical signal processing with very high response times, on the order of femto-seconds. Additionally, the efficiency of the proposed device is very high, allowing the cascading of several devices into more complex systems.

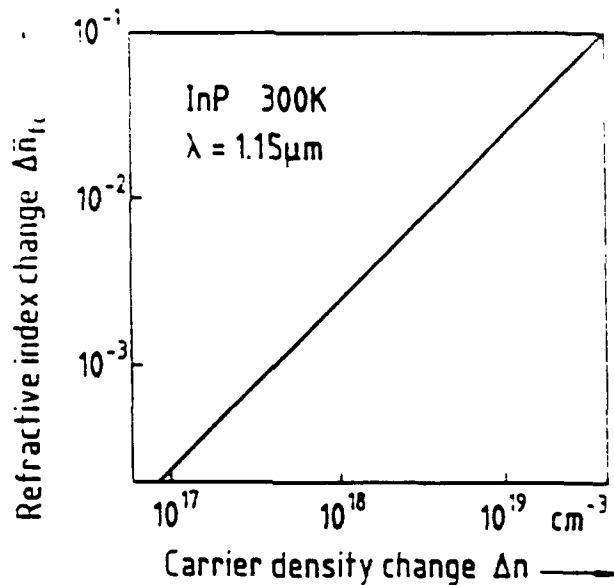


Figure 6
Refractive index variation versus free charge carriers density

3.0 CHANNEL WAVEGUIDE DESIGN AND OPTIMIZATION

One of the key elements in the design of GaAs channel waveguides for the RTDBQW structure is to minimize the overall loss. This loss can be broken into following components:

1. Free carrier absorption loss;
2. Waveguide loss;
3. Coupling loss; and
4. Bending loss.

The free carrier absorption and waveguide losses can be minimized during the design and fabrication of the waveguide. Coupling and bending losses are introduced during the experimental development and testing, and can be minimized through careful implementation.

The free carrier absorption loss is caused by the absorption of free electrons and holes, and is proportional to the carrier concentration (as shown in Figure 7) [12]. In general, the free carrier absorption is linearly proportional to the carrier concentration, and inversely proportional to their mobility.

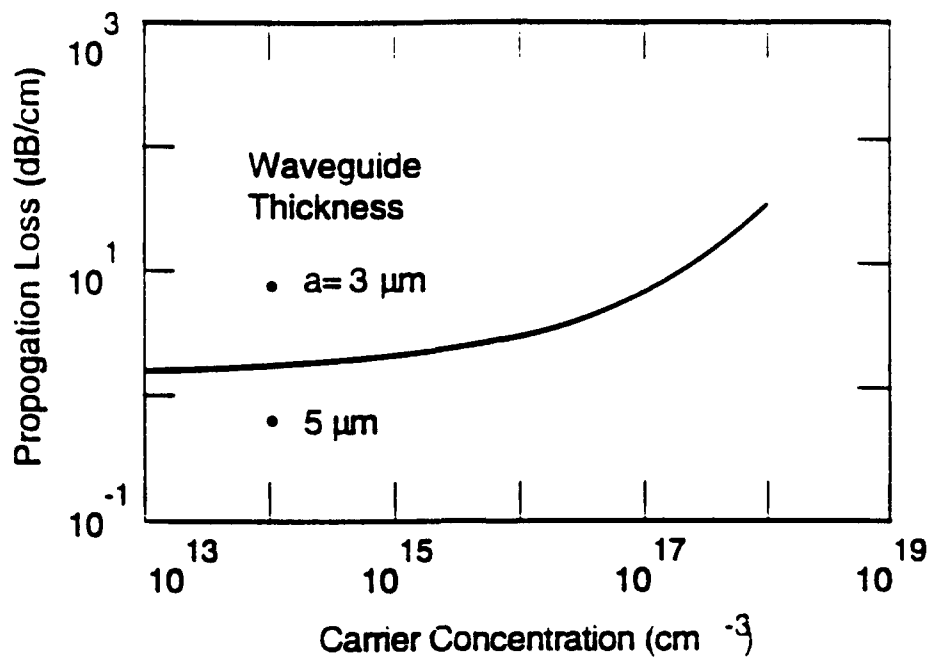


Figure 7
Dependence of the propagation loss as a function of the free carrier concentration in the GaAs ridge waveguide

In order to lower the free carrier absorption loss, low doping density ($<10^{13} \text{ cm}^{-3}$) inside the guiding layer should be maintained. In such a case, the propagation loss can be minimized to approximately 1 dB/cm.

The waveguide loss is a result of penetration of the electromagnetic field into the waveguide cladding. This loss can be minimized by providing high mode confinement in the guiding layer in order to reduce the field penetration into the cladding layer. This is usually achieved by providing relatively thick waveguide and cladding layers between the waveguide layer and the substrate.

There are two methods to achieve strong mode confinement in a waveguide. The first is to make the waveguide layer thicker, and the second is to insert a cladding layer between the guiding layer and the substrate. The waveguide propagation loss is depicted in Figure 8 as a function of the cladding thickness for three different values of waveguide layer thickness [13]. Figure 8 shows the importance of the proper thickness of the cladding layer in the confinement of the guided waves. For cladding thicknesses in the range of $2 \mu\text{m}$, the propagation loss can be reduced to approximately 0.1 dB/cm. The carrier concentration of the substrate is 10^{18} cm^{-3} , and that of the waveguide layer is 10^{14} cm^{-3} .

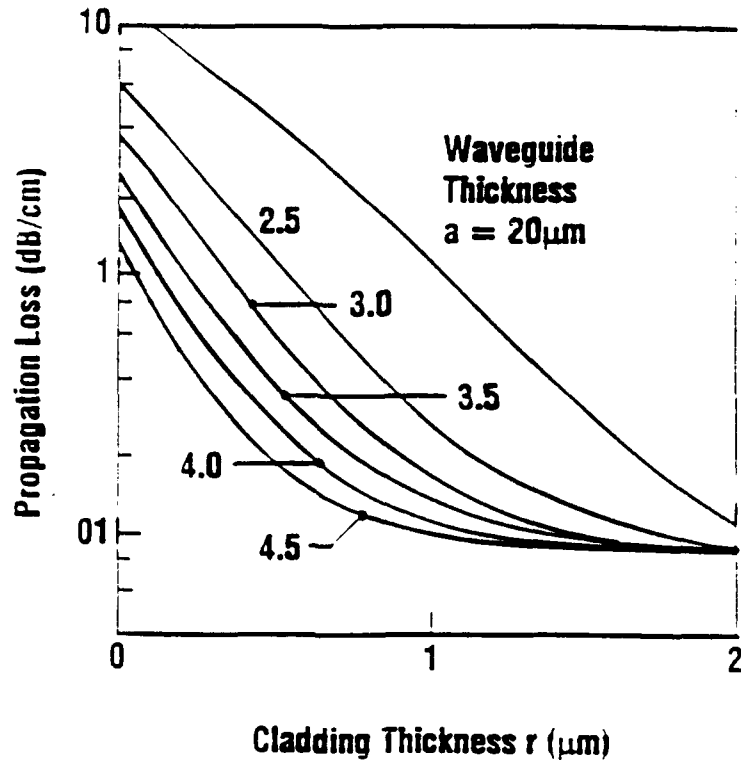


Figure 8
Waveguide propagation loss of the fundamental mode in the ridge waveguide as a function of the cladding thickness for various waveguide thicknesses.

The calculation of the proper cladding and guiding layer thicknesses must be calculated taking into account two factors:

1. Strong confinement of the guided waves in the guided layer (larger values for larger cladding and guiding layer thicknesses).
2. Singlemode operation requires relatively small guided layer thicknesses (most electrooptical integrated optics devices need singlemode operation).

These two requirements are contradictory, and require waveguide structure optimization. For this purpose, we used the WaveDesign™ software. The design parameters given by the WaveDesign™ software are shown in Figure 9, which shows the actual computer screen readout. After considering several options for the waveguide dimensions, the best solution (in terms of minimum propagation loss and preservation of the singlemode operation) was determined as: The waveguide was 7.0 μm wide by 4.0 μm high. Based on the performance of the software simulation, the following waveguide performance characteristics were achieved:

1. A waveguide thickness of more than 4.0 μm minimized the propagation loss to < 0.1 dB/cm.
2. A low concentration of carriers (approximately 10^{13} cm^{-3}) assured a low absorption loss of < 0.5 dB/cm.

3. The combined loss from bending and coupling can be maintained at a total level of 2 dB/cm.

The total loss introduced by the waveguide can be maintained at the low level of 2-3 dB, which will assure the proper optical power budget of the device.

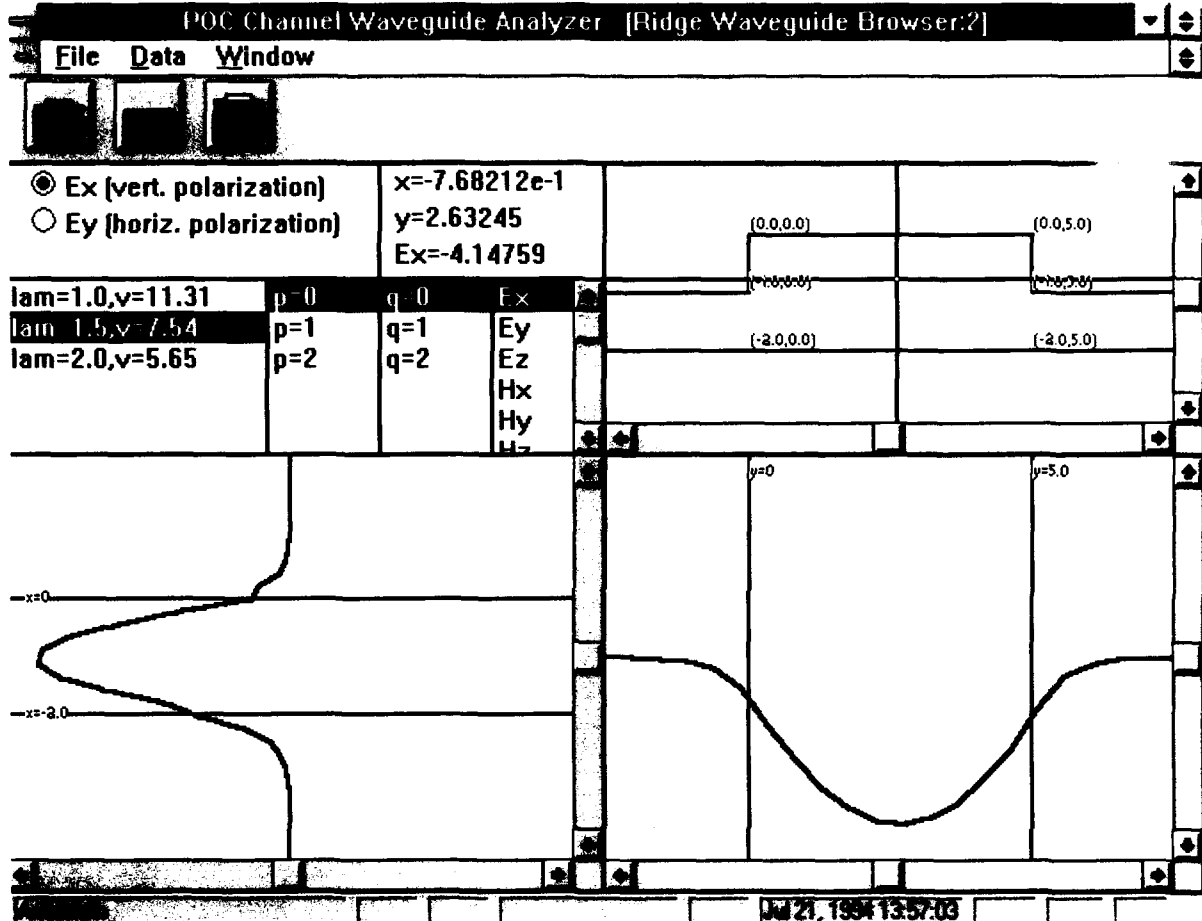


Figure 9
 Computer screen showing field distribution for the optimized simple mode waveguide.

3.1 Design Of Directional Coupling Mach-Zehnder Interferometer

During the course of this Phase I project, POC investigated different electro-optic modulators, including directional couplers, x-switches and Mach-Zehnder interferometers. After careful consideration, we have selected the Mach-Zehnder interferometer as the most suitable for integration with the proposed RTDBQW structure. A conceptual diagram of the Mach-Zehnder interferometer is shown in Figure 10. The input light is divided between two arms *a* and *b*, and propagates parallelly. Each arm is a singlemode waveguide with identical optical pathlengths. Electrooptic modulation in one of the arms will induce a change in the index of refraction in one arm (e.g., *b*), and as a consequence will change the

phase of the incoming light. The phase difference between the two arms will allow us to achieve high on/off intensity modulation depths.

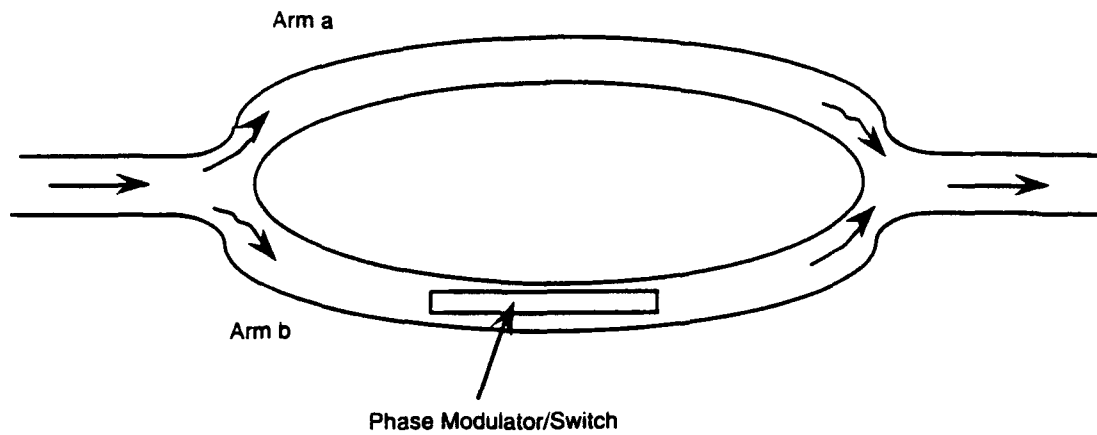


Figure 10

Schematic diagram of Mach-Zehnder interferometer. Arm *b* contains the phase modulator, inducing a phase change in the incoming light through the modulation of the index of refraction in this arm.

Using this interferometric structure, an RTDBQW carrier-induced phase modulation can be converted to an amplitude modulation. The optical transmission of the interferometer is a sinusoidal function of the relative phase shifts between the two optical paths. The output power, P_{out} , is a function of the carrier induced propagation mismatch $\Delta\beta$, where the optical transmission characteristic depends on the normalized interaction length L/l , and the propagation constant mismatch $\Delta\beta$ between the two coupling waveguides is

$$\Delta\beta = \frac{2\pi}{\lambda} \Delta n \quad (18)$$

The induced $\Delta\beta$ phase mismatch results in the modulation of the transfer characteristics. The two waveguides are then merged at another pair of directional couplers.

The output power depends on $\Delta\beta$ and the input power:

$$\begin{aligned} P_{out} &= P_{in} \cos^2 \left[\frac{1}{2} \Delta\beta L \right] \\ &= P_{in} \cos^2 \left[\frac{\pi}{2} \left(\frac{\Delta\beta L}{\pi} \right) \right] \end{aligned} \quad (19)$$

The propagation mismatch $\frac{\Delta\beta L}{\pi}$ is a function of the carrier induced index change. The optical transmission characteristic P_{out} vs. $\frac{\Delta\beta L}{\pi}$ is shown in Figure 11.

The condition for a complete switching on and off of light at the output waveguide is given by

$$\Delta\beta L = \pi \quad (20)$$

By using the difference of the propagation constant, we obtain the following RTDBQW induced complete switching condition:

$$\Delta n = \frac{\lambda}{2L} \quad (21)$$

As an example, for operation at $1.3 \mu\text{m}$, the electrode length required to induce a 180° phase change is around $9.5 \mu\text{m}$ for a 2% carrier induced index change. More than 2% carrier induced index change has been demonstrated at POC.

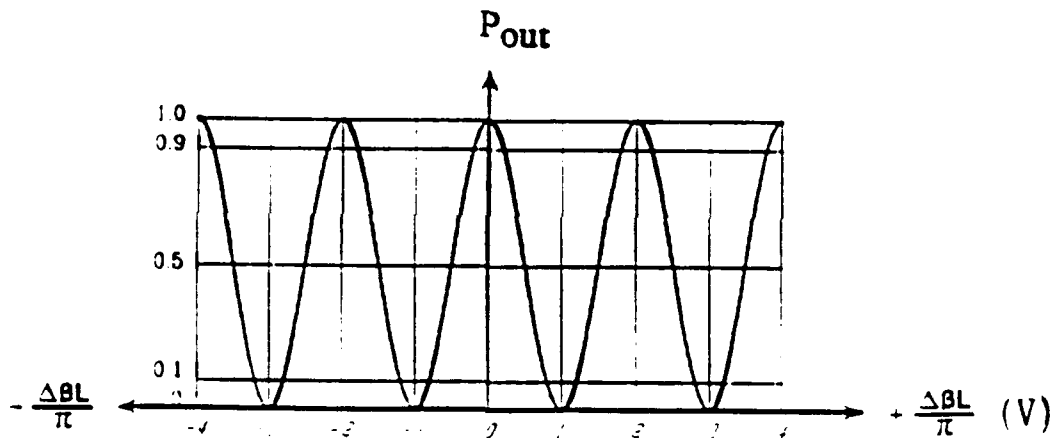


Figure 11
 P_{out} versus $\Delta\beta/\pi$ characteristics of the Mach-Zehnder interferometer.

In this program, a Mach-Zehnder interferometer was fabricated together with the RTDBQW using the several masks shown in Figure 12.

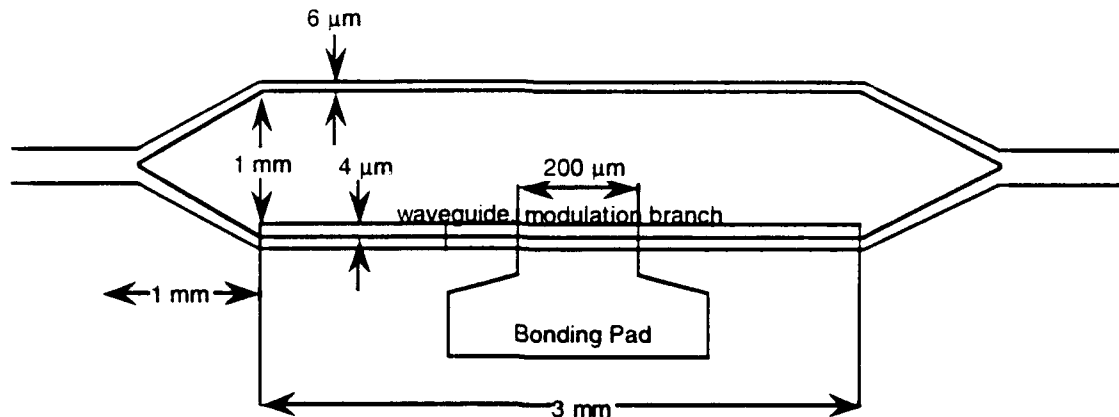


Figure 12
The mask layout used for the fabrication of the Mach-Zehnder interferometer

4.0 WAVEGUIDE FABRICATION

This section provides information on the fabrication of single and multimode waveguides. A waveguide is formed by etching channels into the waveguide material. There are two etching methods, chemical etching (wet etching) and dry etching. The wet etching solution usually consists of two diluted chemicals. One chemical provides material oxidation, such as H_2O_2 . The other chemical removes the oxidized material, and usually an acid. A diluted etchant solution controls the etching rate, which is usually different for different compositions of AlGaAs. To form a good and smooth waveguide for minimum scattering loss, we need to find an etchant with an even etching rate for AlGaAs with different Al compositions. During the Phase I study, we selected the etchant $H_2O_2:H_3PO_4:H_2O=2:6:25$; which met this requirement; the oxide removal agent is H_3PO_4 . The etching rate was around $2 \mu\text{m}/\text{min}$. for fresh mixed solution. Here we emphasize the "Fresh Mix," since the etch rate changes rapidly with the age of the mixture. The etching mask is photoresist, which is usually AZ5214E. Since the side wall scattering of the waveguide is always a problem for low loss waveguides, we needed to minimize the scattering loss by smoothing the side wall. Part of the unsmoothness of the waveguide comes from the pattern transfer from the photomask to the photoresist etching mask, where a thin layer of photoresist (scum) was left during the development. In order to smooth the etching mask, we used an oxygen plasma to descum. The power of the oxygen plasma was 50W, and the descuming time was 10 min. A schematic cross-sectional profile of the waveguide is shown in Figure 13. The etching depth was monitored by a α -step, which has an accuracy of 500 \AA .

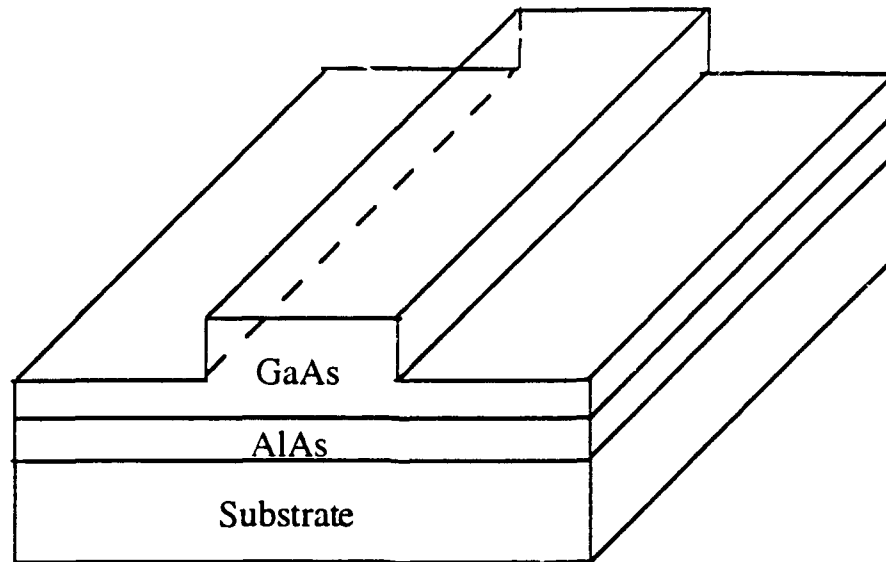
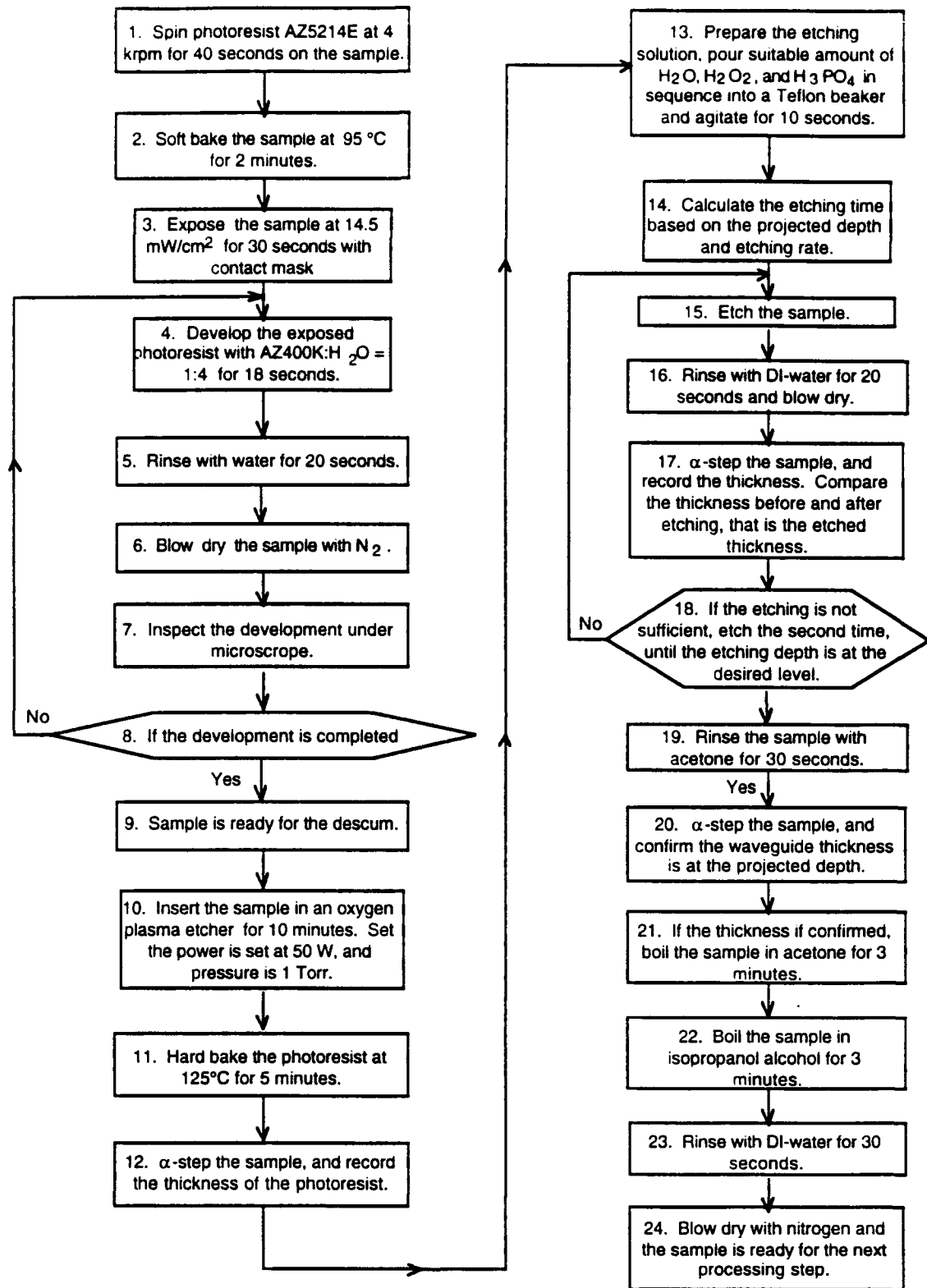


Figure 13
Layer structure of the proposed waveguide

During the Phase I project, POC has optimized the waveguide fabrication procedure by defining each step of the process and verifying it in the final waveguide fabrication. The two main etching methods are presented in more detail below.

4.1 Wet Etching Waveguide Fabrication Method

The wet etching process consists of the following steps. This fabrication method ensures high yield and repeatability in the of waveguide fabrication process.

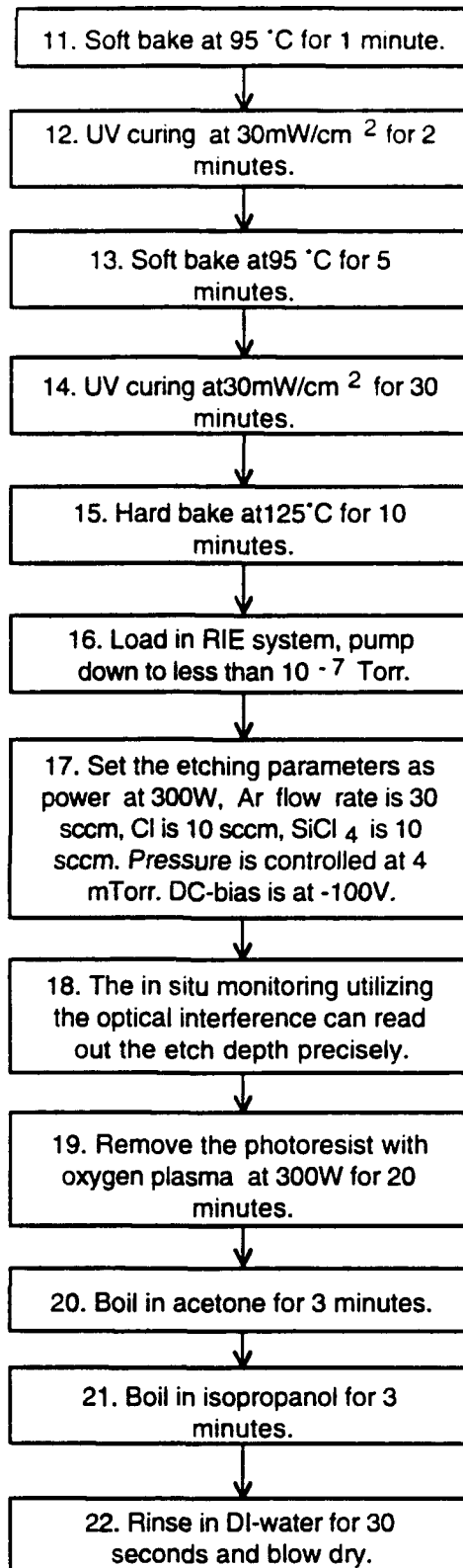


Flow Chart 1
Wet Etching Process

4.2 Dry Etching Waveguide Fabrication Method

An alternative to wet etching is dry etching which may provide a more controllable optical waveguide fabrication process. However, this method requires more sophisticated instrumentation. We used reactive ion etching (RIE) for this purpose, which enabled us to make a waveguide with straight walls with more precise in-situ monitoring.

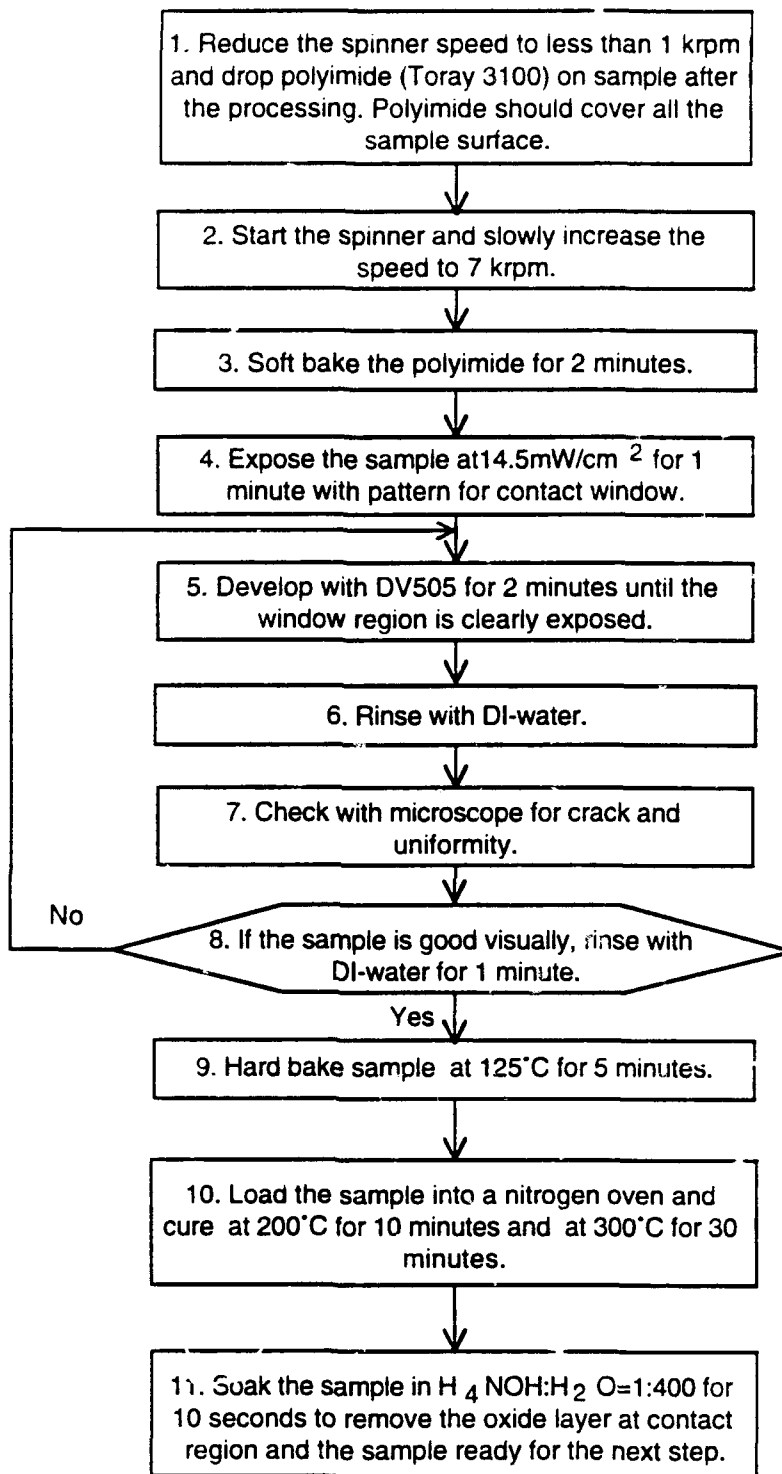
The first 10 steps from the wet etching method were repeated for the dry etching method so here we only present the remaining steps.



Flow Chart 2
Dry Etching Process

4.3 Device Isolation

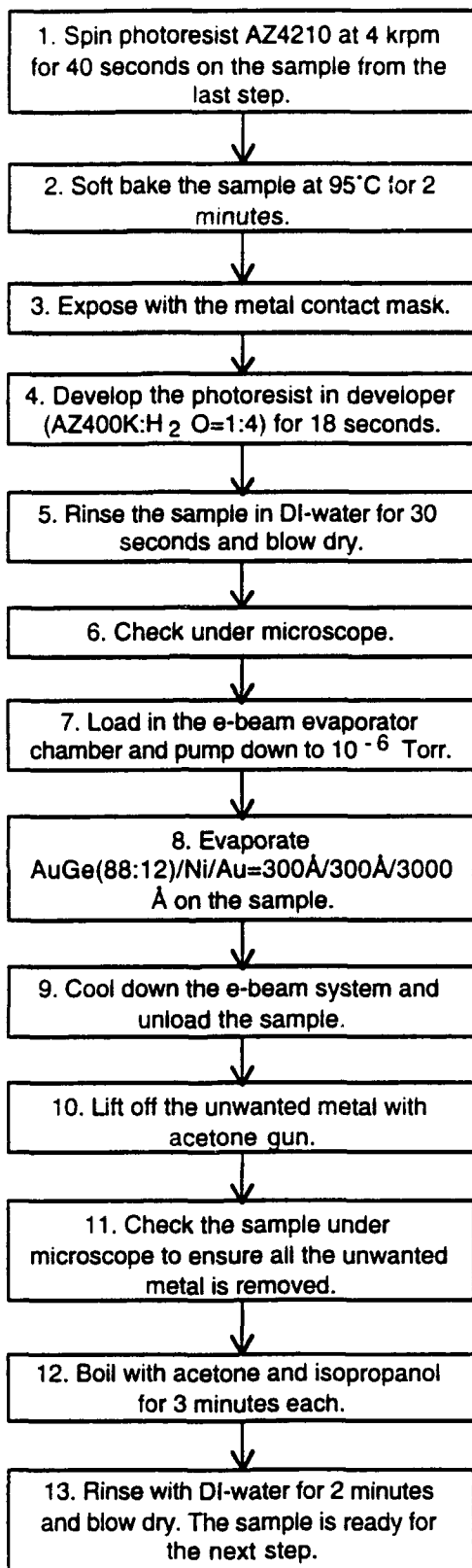
Isolation between the devices is provided by a polyimide layer. The refractive index of the polyimide is 1.3, which is close to the refractive index of air. This will affect the wave propagation in the waveguide. The polyimide we used is a photosensitive material, with the exposed region staying on the sample during UV exposure, and the unexposed region removed during the development. The processing steps are listed below.



Flow Chart 3
Device Isolation Process

4.4 Contact Metal Deposition

Contact metal deposition provided the ohmic contact to the modulation region. The metal chosen was AuGe(88:12)/Ni/Au. The reason for choosing this metal was that Ge diffuses into the n-type GaAs and heavily dopes the material, resulting in a low resistance contact. The processing steps are listed below.



Flow Chart 4
Contact Metal Deposition Process

4.5 Pad Metal Deposition

The metal pad was used for wire bonding to the fixture for testing. For this application, the metal must be strongly adhered to the polyimide. Thus, we used Cr/Au for the pad metal, where Cr acts as a "glue" to polyimide, and the Au layer provided Au wire bonding. The processing steps are the same as the previous contact metal deposition, except the metal material. The thickness of the metals is Cr/Au=300Å/3000Å.

4.6 Backside Metal Deposition

The backside metal deposition provided another electrode for the two-terminal device. The backside thinning and polishing was performed before the metal deposition. The sample must be thinned to less than 120 μm for a proper cleaving. Here, the samples were thinned using an Al₂O₃ powder and polished by bleach with polishing pads. The backside metal is the same as the contact metal.

4.7 Metal Alloying

The contact metals needed to be alloyed before testing. Alloying provides the ohmic contacts to the device. The alloying condition was 400°C for 2 minutes. The contact resistivity was $5 \times 10^{-6} \Omega \text{cm}^2$.

4.8 Post Processing

After the alloying, the processing of the device is essentially finished. Before testing, we cleaved the sample to the individual devices for testing. The cleaving is along the natural crystallographic orientation, which provides a perfect facet to the waveguide. The cleaving is very important, since the coupling of the light into the waveguide depends on the facet quality of the waveguide.

5.0 DEVICE CALIBRATION AND TESTING

There are two calibrations needed for the proposed structure. One is the doping calibration and the other is the thickness calibration. The precise thickness control is essential for some modulators that work close to the cutoff condition. The doping calibration can be performed using the Hall measurement. The Hall measurement also provides the mobility information of the material; by comparing the measured mobility and published data, we can determine the quality of the material. This is very important for this kind of device, since the coherent length (proportional to mobility) of the carriers has to be long enough for quantum tunneling to occur. The thickness calibration can be performed based on the reflectance of the structure. Reflectance is the reflectivity spectrum of the material. A program was developed based on the refractive index of the AlGaAs system. By measuring the reflectance of the structure and comparing this with the simulation curve, the thickness variation of each layer was calculated. In this way, we are able to fabricate a waveguide that operates close to the cutoff condition. Figure 14 shows the simulated reflectance of the structure.

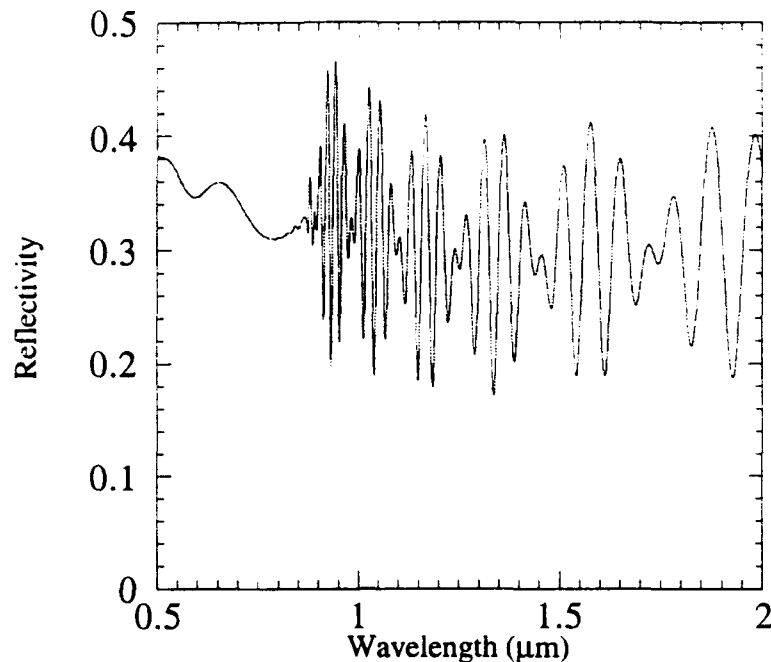


Figure 14
Simulated reflectance of the proposed structure

6.0 POTENTIAL APPLICATIONS

The hybrid modulator/switch developed in this program will fit very well in future computer networks, as well as in the multimedia "Information Superhighway." It will also be an essential building block in optical signal computing and processing systems. POC's RTDBQW diode, based on the advanced high speed multiple quantum well technology, can be fully integrated with OEICs, and achieve much higher speed performance than the existing devices. The potential of devices based on this technology can provide tremendous benefits to both the commercial and military sectors.

6.1 All-Optical Synchronous Multiple Access Networks

The massive signal processing requirements of "Information Superhighway" applications will require extremely high bandwidth channels and high speed devices. To this end, the high bandwidth-distance product of optical fiber for long haul digital communications has already been demonstrated. However, using an optical fiber as a high bandwidth channel is, by itself, insufficient to implement high capacity networks. The capacity of the channel is limited by the processing speed of the associated electronic circuitry. The state-of-the-art in electronic technology yields maximum processing speeds of approximately multi-gigahertz. On the other hand, by using POC's ultra high speed (~picosecond) RTDBQW switches, much higher processing speeds can be achieved.

One of the applications is for a serial time division multiplexer (TDM) using POC's RTDBQW switches, as shown in Figure 15. Here, M fixed delay lines of length $\tau \cdot c/n$ are connected serially with 1×2 RTDBQW high speed optical switches. The slot selector unit selects the desired time delay nT and routes the signal through the $M \times 1$ optical switch. Thus, the optical data signal can be multiplexed into the correct destination time slot. Using this architecture, a fixed assignment TDMA (Time Division Multiple Access) scheme can be achieved.

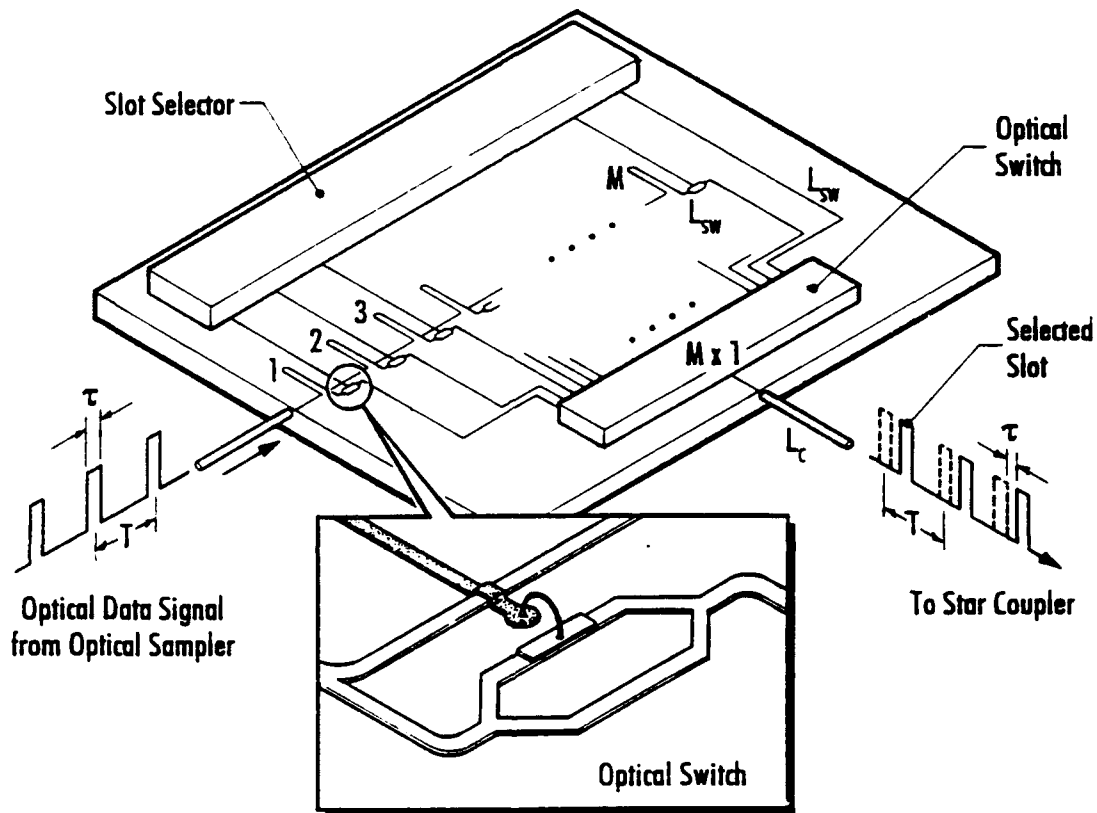


Figure 15

The optical data signal is split into N different delay paths. The code selector selects the paths corresponding to the chosen code sequence. The paths are recombined at the optical combine. L_{SW} is the switch excess loss.

7.0 PHASE I CONCLUSIONS

A high speed RTDBQW diode integrated with a Mach-Zehnder interferometer has been designed using bandgap engineering in this Phase I program.

Based on the anticipated performance of the RTDBQW device, we have determined that high speed optical signal processing can be realized. In order to explore the potential for OEICs, the development of low loss singlemode waveguides with propagation losses of less than 1 db/m was achieved. These results are very positive and encouraging, because

a variety of integrated optical components, including optical switches, modulators, detectors, signal and image processors, and backplane optical interconnects can be realized based on this innovative technology. In Phase II, a high speed, highly sensitive RTDBQW device will be applied to SONET/ATM networks.

8.0 PHASE II RECOMMENDATIONS

During the Phase I program realization, it became obvious that the design of a high speed RTDBQW diode is only the first step to a far more ambitious goal. This goal is the design and prototype demonstration of an ultra-high speed all-optical switch for communication applications. Such switches can be applied to high throughput asynchronous transfer mode (ATM) systems as packet selectors and routers. Such issues as the integration of a large number of RTDBQW switches in 1D and 2D arrays will be investigated during the Phase II program. Packaging issues will be critical in the final commercialization effort. Another aspect of the proposed device is its integration with optical components and electronic driving circuits in hybrid OEIC modules. We will also analyze the integration capabilities of POC's RTDBQW switch with other OEIC components, such as optical detectors, modulators, and lasers. Higher integration can offer larger bandwidth for optical computing, especially for multi-gigahertz bandwidths.

Our Phase II effort will also concentrate on high speed network issues, where we will analyze the parameters for the ATM networks, including the maximum data rate, jitter, SNR, BER, and the entire electrical and optical power budget.

9.0 REFERENCES

1. Y. Sato and K. Sato, "Virtual Path and Link Capacity Design for ATM Networks," *IEEE J. on Sel. Areas in Commun.* Vol. 9, No. 1, Jan. 1991, pp. 104-111.
2. J.J. Bae and T. Suda, T., "Survey of Traffic Control Schemes and Protocols in ATM Networks," *Proc. IEEE*, Vol. 79, No. 2, Feb. 1991, pp. 170-189.
3. A. Zaslavsky, V.J. Goldman, D.C. Tsui, and J.E. Cunningham, "Resonant Tunneling and Intrinsic Bistability in Asymmetric Double-Barrier Heterostructures," *App. Phys. Lett.* 53(15), 1998, pp. 1408-10.
4. T. Wei, S. Stapleton, and E. Berdo, "Equivalent Circuitry and Capacitance of Double Barrier Resonant Tunneling Diode," *J. Appl. Phys.* 73(3), 1993, pp. 829-834.
5. Y. Fu and M. Willander, "The Interaction between Electron and Photon Localized in a Double-Barrier Resonant Tunneling Diode," *J. Appl. Phys.* 75(5), 1993, pp. 3264-3269.
6. C. Van Hoof, G.S. Raymond, and G. Borgus, "Giant Optical Bistable Behavior Using Triple-Barrier Resonant Tunneling Light-Emitting Diodes," *App. Phys. Lett.* 63(17), 1993, pp. 2390-2392.
7. E. Walak, et al., "The Design of GaAs/AlAs Resonant Tunneling Diodes with Peak Current Densities over 2×10^5 A cm⁻²," *J. Appl. Phys.* 69(5), March 1, 1991, pp. 3345-3350.

8. K.J. Ebeling, Integrated Opto-electronics, Springer-Verlay, Berlin, 1992.
9. S. Adachi, "GaAs, AlAs and $\text{Al}_x\text{Ga}_{1-x}\text{As}$: Material Parameters for Use in Research and Device Application," J. Appl. Phys. **58**(3), 1985, pp. R1-R29.
10. Y. Hu and S. Stapleton, "Sequential Tunneling versus Resonant Tunneling in a Double-Barrier Diode," J. Appl. Phys. **73**(12), 1993, pp. 8633-8636.
11. N. W. Ashcroft, et al, Solid State Physics, (Cornell University, Ithaca, NY, 1976).
12. W.G. Spitzer and J.M. Whelan, Phys. Rev., V. **114**, p. 59 (1959).
13. Hiroaki Inoue, Kenji Hiruma, Koji Ishida, Takahiro Asai, and Hiroyoshi Matusmura, J. of Lightwave Tech., V. **LT-3**, p. 1270 (1985).